An Avalanche-to-Streamer Transition Criterion for Overstressed Breakdown on a Rising Slope

Timothy Wong, *Member, IEEE*, Igor Timoshkin, *Senior Member, IEEE*, Scott MacGregor, *Senior Member, IEEE*, Mark Wilson, *Member, IEEE*, Martin Given, *Senior Member, IEEE*

***Abstract*—The Meek-Raether criterion underpins much of the current physical understanding of gas breakdown. The classical kinetic approach estimates the moment of transition from Townsend's avalanche to a streamer discharge, and has very often been used as a means of explaining experimental breakdown results. The Meek-Raether criterion holds great predictive power for the design of gas insulated systems, owing to its reasonable accuracy that has withstood the test of time. However, with the advent of pulsed power technology which often involves fast-rising and non-standard waveshapes applied to complex (nonuniform) electrode topologies, the limitations of the method have been made increasingly apparent. In this work, the avalanche-to-streamer transition criterion has been theoretically revisited for fast-rising pulsed breakdown, particularly for overstressed breakdown occurring on a rising voltage slope. Based on the simplified transport of a Gaussian-distributed electron density, mathematical analyses unveils the time-dependent nature of the electron growth rates and their dependence on the voltage slope. Explicit expressions for the breakdown voltage and formative breakdown time, under the assumption of no statistical time lag, as a function of the rate-of-rise have further been derived for the limiting case of a non-attaching and non-diffusive gas. From this, it was found that electron diffusion may be an important consideration for pulsed breakdown, and an approximate condition separating the diffusion-dominated regime and where diffusion can be neglected is suggested. The novel analytical approach is also shown to be capable of recreating the upward shift of Paschen's curve with increasing rate of voltage rise, validated against both simulation and experimental data. Furthermore, the predicted field-time breakdown scaling relationship is also shown to describe observed experimental trends well; as do its predictions for the streamer initiation time compared to hydrodynamic simulations. The results may be significant for the future development of gas insulated power and pulsed power equipment, and advances the fundamental understanding of fast transient breakdown processes.**

***Index Terms*—electron avalanche, streamer discharge, electrical breakdown, gas discharge, pulsed power technology, ionization, mathematical modeling**

I. Introduction

THE pioneering work of Townsend [1], Paschen [2], Meek [3], Loeb [4]–[6], and Raether [7] revolutionised the collective understanding of gaseous breakdown. The fundamental processes driving gas breakdown underpins the design of all gas insulated high voltage (HV) systems. Examples include power transmission, distribution, and protection apparatus; pulsed power machines; novel plasma-based technologies; or equipment for high energy physics research. The rapid advancement of HV technology shows no indication of slowing, pushing insulating systems to their limit. For example, novel pulsed power systems operating using nanosecond rising impulses (and often under non-standard electrode geometries, involving non-standard materials) imposes substantial transient electrical stress on insulating components—far above what would have been possible mere decades before. However, many classical breakdown models are still widely in use today, with some indication that they are beginning to be outpaced by technological advances.

The subject of the present work is the ubiquitous Meek-Raether avalanche-to-streamer transition criterion (often just Meek criterion), which for completeness, originates from following Townsend's [1] analysis based on the first-order differential equation

$$\frac{\partial N_e}{\partial \ell} = \bar{\alpha} N_e, \tag{1}$$

where N_e is the number of electrons in an avalanche, $\bar{\alpha}$ is the effective ionisation coefficient, and $d\ell$ is a differential distance in the direction of electron transport. It is hereby noted that standard SI units are assumed throughout this work, unless otherwise stated. The solution to (1) predicts exponential growth or decay of the electron number depending on the nature of $\bar{\alpha}$,

$$N_e = N_0 \exp\left(\int_\ell \bar{\alpha}\left[E(\ell')\right]\ d\ell'\right), \tag{2}$$

where N_0 is the initial condition. The exponent of (2) determines the growth rate of the avalanche, commonly assigned the letter K and may be referred to as the *ionisation integral*. Since the effective ionisation frequency, $\bar{\nu}$, may also be expressed as $\bar{\nu} = \bar{\alpha} v_d$ with v_d being the drift velocity, the integral may equivalently be expressed as a function of time, t, according to

$$K = \ln\frac{N_e}{N_0} = \int_\ell \bar{\alpha}\left[E(\ell')\right]\ d\ell' = \int_t \bar{\nu}\left[E(t')\right]\ dt', \tag{3}$$

which reflects the spatial and temporal nature of the avalanche growth. For an avalanche to transition into a streamer, it is well known that Meek estimated the value of K to be 18–20 for atmospheric air under a uniform electric field [3], which agreed with empirical estimates by Raether [7]. This baseline

T. Wong was supported in part by the Engineering and Physical Science Research Council (EPSRC) under grant number EP/T517938/1.

Manuscript received Month XX, 2024; revised Month XX, 2024.

value has since been extensively scrutinised and found to be a very reasonable approximation in many cases [8], [9].

However, the increasing interest in nonuniform field geometries, novel gases/gas mixtures, and complex time-varying voltage waveforms has highlighted the limitations of the Meek criterion. Many authors have used this theory to fit the parameter K to experimental breakdown data, finding that K depends highly on the specific experimental conditions, see for instance, [10]–[15].

The phenomenological nature of the value of K renders it difficult to make conclusive comparisons between breakdown data or to be certain about the dependencies of K. On the other hand, while Meek's original theoretical analysis [3] was sound, it was limited by the assumption of a constant and uniform electric field, among others. An improved analysis was conducted by Montijn and Ebert [9], who mathematically modelled the avalanche growth using an evolving Gaussian distribution of electrons, showing that electron diffusion can have significant influence on the avalanche development under certain conditions.

In this work, focus was placed on modelling the avalanche development and transition under a time-varying applied field. Of particular interest are fast-rising impulsive waveforms and overstressed breakdown occurring on the rising slope, relevant to pulsed power science and technology. In the field of pulsed breakdown, there exists numerous (and growing) sets of well-established experimental data, but comparatively few studies investigating novel theoretical descriptions of the breakdown process. To do so, the present work begins with the approach taken by Montijn and Ebert [9], then extending it to explicitly incorporate time-dependency. The new mathematical model is then subjected to theoretical analysis, and the predictions of the new model have been compared to practical pulsed breakdown experimental data.

II. Mathematical Model

This section describes the formulation of the mathematical model. Sections II-A and II-B firstly presents the full set of equations for the simplified transport of a Gaussian distributed electron cloud and the criterion for streamer transition. Section II-C follows to present an approximation to the full model for linearly increasing voltages. Subsequent analysis and discussion, including that of further approximations allowing the derivation of closed solutions under a limiting case, are presented in Section III.

A. Gaussian Electron Cloud

The approach follows a similar approach to [9] by considering an initial Gaussian distribution of electrons, modelled here in spherically-symmetric coordinates as

$$n_e(r,t_0) = n_0(t_0)\exp\left(-\frac{r^2}{2\sigma_0^2}\right), \tag{4}$$

where $n_e(r,t)$ is the electron density, $n_0(t)$ is the time-dependent peak value of the Gaussian, σ_0 is the initial spread of the Gaussian, and r is the radial coordinate. It was firstly assumed that this initial electron "cloud" at t_0 undergoes constant and field-independent diffusion, characterised by the diffusion constant D_e. It is remarked that this assumption may not always be valid as D_e is, in general, field dependent, but it is nonetheless applied for simplicity. Section V-A encloses further discussion on this assumption and on its limitations. In this case, Fick's law of diffusion dictates that the initial electron cloud of (4) will evolve like (see Appendix A)

$$n_e(r,t) = n_0(t)\frac{\left(2\pi\sigma_0^2\right)^{3/2}}{\lambda_2^3}\exp\left(-\frac{r^2}{\lambda_1^2}\right), \tag{5}$$

where λ_1 and λ_2 are time-dependent and related to the diffusion length:

$$\begin{aligned}\lambda_1 &= \sqrt{2\sigma_0^2 + 4D_e t},\\ \lambda_2 &= \sqrt{2\pi\sigma_0^2 + 4\pi D_e t},\end{aligned} \tag{6}$$

and with the overall expression of (5) describing the broadening of the Gaussian as the electron density diffuses outward, resulting also in the reduction of the peak magnitude with time. Counteracting this diffusive reduction is collisional ionisation which was considered to affect the peak magnitude of the Gaussian cloud. Following the growth equation (1), the Gaussian peak grows according to the ordinary differential equation:

$$\frac{\partial n_0(t)}{\partial t} = \bar{\alpha}\left[E(t)\right] v_d\left[E(t)\right] n_0(t), \tag{7}$$

where the drift velocity $v_d\left[E(t)\right] = \mu_e\left[E(t)\right]E(t)$ with μ_e being the electron mobility, and where E is the externally applied (and assumed uniform) field. Emphasis is placed on the functional dependence on t for the electric field and transport parameters.

The spatial development of the avalanche was modelled assuming that the Gaussian cloud translates along a single direction at drift velocity, such that the distance travelled, $\delta(t)$, of the cloud evolves like

$$\frac{\partial \delta(t)}{\partial t} = \mu_e\left[E(t)\right]E(t). \tag{8}$$

Then with motion in, for example, the Cartesian x-axis would result in the following definition for coordinate r when applying a Cartesian to spherical transform:

$$r = \sqrt{\left[x-\delta(t)\right]^2 + y^2 + z^2}. \tag{9}$$

It is remarked, however, that if the model were to be used assuming electrodeless breakdown, or where the interelectrode gap distance is greater than the critical streamer transition distance, tracking the location of the Gaussian is not strictly necessary. This is because the derivation of the avalanche-to-streamer transition criterion is based only on the magnitude of the electron density and on its induced field.

B. Streamer Transition Criterion

Maintaining the Gaussian form over the course of its transport was an important assumption applied to the present

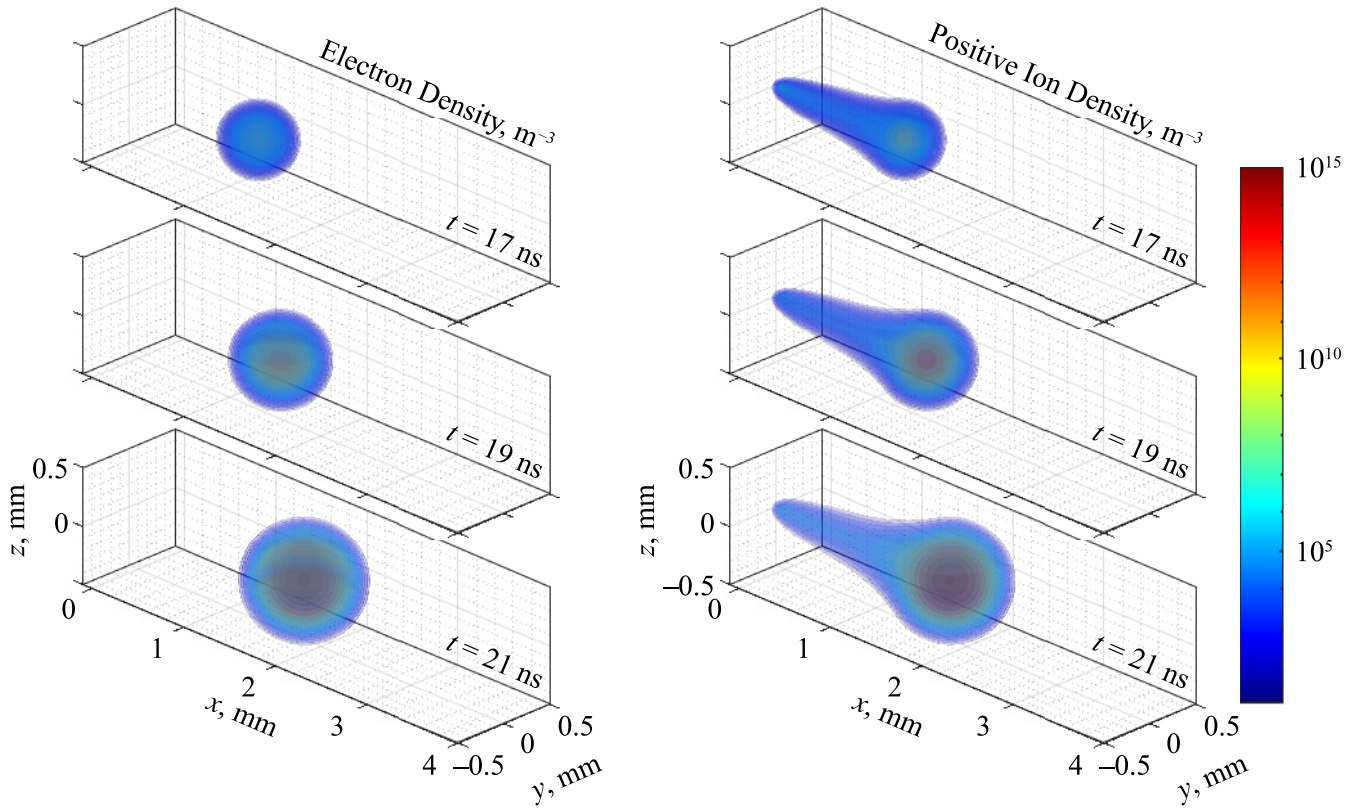

Fig. 1. Volumetric rendering of the estimated (left) electron density (right) positive ion density of an electron avalanche developed across a 4 mm air gap with 0.5 kV/ns applied ramp voltage, at t = 17, 19, and 21 ns. This figure is from the numerical solution of the full model (4)–(12).

model, as a closed-form analytical solution for the electron-induced electric field exists for this distribution, given by:

$$E_e(r,t) = \bar{e}n_0(t)\frac{\left(2\pi\sigma_0^2\right)^{3/2}}{4\pi\varepsilon}\times \left[\frac{1}{r^2}\mathrm{erf}\left(\frac{r}{\lambda_1}\right) - \frac{2}{r\lambda_1\sqrt{\pi}}\exp\left(-\frac{r^2}{\lambda_1^2}\right)\right], \quad (10)$$

where $\bar{e}$ is the elementary charge, ε is the permittivity, and erf is the error function. While Meek originally considered the moment of transition to be when the charge-induced field became equal to the applied field, a more general approach was taken as in [9]. Since an exact value of field necessary for transition is not known (and may vary depending on exact conditions), the more general condition of

$$\max_{r,t} E_e(r,t_b) = f \cdot E(t_b) \quad (11)$$

was instead used, where $f \cdot E(t_b)$ is an arbitrary fraction of the applied field, and where t_b is the time of breakdown. In [9], a value of f = 1.03 (3% enhancement at the avalanche front) was found to be reasonable based on simulated data. It follows that the set of equations (4)–(10) can be solved numerically to obtain the moment that the condition (11) is satisfied, providing the breakdown time t_b, the corresponding breakdown field, E_b, and if applicable, the breakdown voltage V_b.

At this point it is important to note that the positive ions resulting from collisional ionisation have not been considered. This is primarily because the ions left in the wake of an avalanche cannot be assumed to maintain a Gaussian form, and thus would render an analytical description of the ion-induced field highly nontrivial. It is remarked that the positive ion density, $n_+(r,t)$, can be computed numerically by solving

$$\frac{\partial n_+(r,t)}{\partial t} = \max\left(\frac{\partial n_e(r,t)}{\partial t}, 0\right), \quad (12)$$

but only when under the assumption that positive ion production is solely due to collisional ionisation, and that no other process (e.g., recombination, photoionisation) is present that would otherwise affect the positive ion density. While the electric field arising from the ion density (12) has no simple solution, (12) is nevertheless useful for visualisation purposes. To illustrate, Figure 1 shows an electron avalanche according to (4)–(12), including electron and positive ion densities that develop under a ramp voltage rising at 0.5 kV/ns in a 4 mm air gap, rendered in 3D. The volumetric rendering of the avalanche is in qualitative agreement with the classical "teardrop" shape as often used to represent avalanches [16], [17]. It also agrees with those originally imaged in cloud chambers [7], and more recently, simulated using kinetic methods [18].

C. An Approximation for Ramp Electric Fields

The full model comprises equations (4)–(11), the numerical solution of which can be sought for arbitrary $E(t)$ and given functions for the ionisation coefficient and mobility. In this section, however, it is shown that with the help of empirical

fitting expressions, a closed form solution to (10) can be found for linearly increasing electric fields. This is of particular relevance to many pulsed power systems that operate in the overstressed regime, such that breakdown always occurs on the rising slope of an impulse.

The maxima of (10) cannot be found in closed form, however, as explained in [9], the position where $r = \lambda_1$ approximates the location of the field maximum, resulting in the expression

$$E_{e,max}(t) \approx \frac{\bar{e}n_0(t)}{4\pi\varepsilon}\frac{\left(2\pi\sigma_0^2\right)^{3/2}}{\lambda_1^2}\left[\mathrm{erf}(1) - \frac{2}{e\sqrt{\pi}}\right]. \quad (13)$$

It remained that analytical solutions must be sought for the peak electron density (7), which necessitated expressions for the transport parameters $\bar{\alpha}(t)$ and $\mu_e(t)$ such that the product of $\bar{\alpha}(t)\mu_e(t)E(t)$ is time-integrable. Note that the functional dependence on $E(t)$ has been changed simply to t here for brevity, considering that the field is dependent only on time, imparting a time dependence to the transport parameters. In general, no exact expressions exist for such parameters and empirical formulae are more often used when using transport parameters in, for example, numerical simulations. However, approximate solutions can be obtained by assuming $\bar{\alpha}(t)$ and $\mu_e(t)$ can be fit using the commonly-used functions:

$$\bar{\alpha}(t) \approx A_\alpha \exp\left[-\frac{B_\alpha}{E(t)}\right] - C_\alpha, \quad (14)$$

$$\mu_e(t) \approx A_\mu E(t)^{-B_\mu}, \quad (15)$$

where A_α, B_α, C_α, A_μ, and B_μ are constant coefficients unique to the gas type, see for example [8]. This of course means that this approximation is only valid within the range where the above coefficients are also valid. As the approximation here is for linearly increasing electric fields, $E(t)$ therefore has the form

$$E(t) = \mathcal{D}t, \quad (16)$$

where the symbol $\mathcal{D}$ is the rate-of-rise of the electric field. Combining (14), (15), (16) and absorbing the constants, one finds that (7) can be expressed as the separable equation

$$\frac{\partial n_0(t)_{ramp}}{\partial t} = t^{k_1-1}\left[k_2\exp\left(-\frac{k_3}{t}\right) - k_4\right]n_0(t)_{ramp}, \quad (17)$$

where constants k_{1-4} have the definitions

$$k_1 = 2 - B_\mu, \qquad k_2 = A_\alpha A_\mu \mathcal{D}^{k_1-1},$$
$$k_3 = B_\alpha/\mathcal{D}, \qquad k_4 = A_\mu C_\alpha \mathcal{D}^{k_1-1}, \quad (18)$$

and which can be shown to have the solution

$$n_0(t)_{ramp} = n_0(t_0)\exp\left[k_2 k_3^{k_1}\Gamma\left(-k_1, \frac{k_3}{t}\right) - \frac{k_4}{k_1}t^{k_1}\right], \quad (19)$$

where $\Gamma(a,t)$ is the upper incomplete gamma function with the definition

$$\Gamma(a,t) = \int_t^\infty \xi^{a-1}e^{-\xi}\, d\xi. \quad (20)$$

Application of the condition (11) with equations (13) and (19) comprise the approximate analytical solution for ramp voltage breakdown, which can be obtained without the use of numerical methods like before. In the section that follows, analysis conducted on the obtained expressions is presented.

III. Theoretical Analysis and Results

A. The Ionisation Integral, K

Equation (19) provides new perspectives on the avalanche development processes during a rising voltage slope, as it relates the growth of the electron density to the gas transport parameters and to the time-increasing field. It is useful to compare (19) to the standard exponential solution in the case where the applied field is constant, for which the reader is reminded takes the form

$$\bar{n}_0(t) = n_0(t_0)\exp\left(\nu t - \nu_a t\right), \quad (21)$$

where ν and ν_a are the ionisation and attachment frequencies, respectively. The net rate of electron growth or decay is therefore determined by the balance between ionisation and attachment. The solution under ramp energisation takes the same form, and comparison between (21) and (19) shows that the constant ionisation and attachment rates in (21) that originally produced exponential growth at constant rate, are now considerably more complex, with

$$\nu t \to k_2 k_3^{k_1}\Gamma\left(-k_1, \frac{k_3}{t}\right) = \mathcal{I}(t),$$
$$\nu_a t \to \frac{k_4}{k_1}t^{k_1} = \mathcal{A}(t), \quad (22)$$

such that the exponent is no longer linear with time, reflecting the time-varying nature of the ionisation and attachment frequencies with increasing field. The symbols $\mathcal{I}$ and $\mathcal{A}$ have been adopted to indicate the rates of growth (due to ionisation) and decay (due to attachment) of the electron density, respectively. The upper incomplete gamma function in (19) dictates that the electron growth rate due to ionisation increases slowly at first, slower than that of the linear νt (i.e., constant ν under a static field), but increases rapidly to grow faster than νt (with power-law like behaviour). This is counteracted by attachment, which according to (22) now follows a power law. The exact nature of the net growth rate is of course dependent on the constants k_{1-4}, which correspondingly means that the rate-of-rise $\mathcal{D}$ also has influence. This behaviour is believed to reflect the slow avalanche development at the beginning of the rising slope, which then rapidly increases due to the increase in both voltage and the corresponding electric field.

It follows from (19) that an effective value for the ionisation integral, K, in this case is also a function of diffusion, D_e, and may be written

$$K_{ramp}(t) = \ln\left[\frac{n_e(0,t)}{n_0(t_0)}\right] + \frac{3}{2}\ln\left(1 + \frac{2D_e t}{\sigma_0^2}\right), \quad (23)$$

such that in the zero-diffusion limit, K_{ramp} reduces to the standard definition of K. The second term of (23) shows the increase of the K value with increasing diffusion, an indicator that diffusion delays the development of sufficient electrons to distort the applied field (see also the discussion within Section V-A). This therefore increases K at the time of breakdown, as similarly concluded in [9].

B. Explicit Solutions for Zero-diffusion and Non-attaching Limit

It is well known that the impulsive breakdown strength of gas is higher than that of the static breakdown strength, and that it increases with faster-rising voltages. However, the physical mechanism behind this increase is not yet clear and would benefit from further analysis. To further understand the effect of $\mathcal{D}$ on the avalanche development process, this section deals with the limiting case where electron diffusion and attachment are assumed negligible. Both of these mechanisms tend to reduce the electric field magnitude induced by the avalanche—the former reduces the charge density gradients near the front, while the latter results in an overall reduction of the electron density, effectively delaying the moment of field distortion. It is shown in the following derivations that explicit solutions for t_b, E_b, and V_b can be obtained under these assumptions, providing closed-form expressions that allow the dependence of E_b on rate-of-rise to be explained. It should be noted that in general, diffusion may not be negligible and is dependent on the exact conditions of breakdown. In Section V-A, an approximate condition to the applicability of the zero-diffusion condition to discharges under fast-rising voltages is derived, and it is further hypothesised that the effective K value for overstressed breakdown exhibits a local minimum as a function of $\mathcal{D}$ due to diffusion. Despite this, the introduction of a physically-based fitting factor allows the expressions obtained within this section to be directly applied as a predictive model in the overstressed breakdown regime, which is supported by comparison to experimental data in Section IV.

To show the explicit dependence on $\mathcal{D}$, it is useful to introduce

$$\gamma_1 = A_\alpha A_\mu B_\alpha^{k_1}, \qquad \gamma_2 = \frac{A_\mu C_\alpha}{k_1}, \tag{24}$$

which allows the redefinition of the ionisation and attachment rates, $\mathcal{I}(t)$ and $\mathcal{A}(t)$ of (22), to a more convenient form involving $\mathcal{D}$:

$$\mathcal{I}(t) \to \frac{\gamma_1}{\mathcal{D}}\Gamma\left(-k_1, \frac{B_\alpha}{\mathcal{D}t}\right), \qquad \mathcal{A}(t) \to \frac{\gamma_2}{\mathcal{D}^{1-k_1}}t^{k_1}. \tag{25}$$

By then introducing the non-diffusive and non-attaching assumption ($D_e = C_\alpha = 0$), the approximate maximum electron-induced field according to (13) may be written in the form

$$E_{e,max}^{D,C_\alpha=0} = C_0 \exp \mathcal{I}(t), \tag{26}$$

where C_0 is a constant given by

$$C_0 = \frac{\bar{e}n_0(t_0)}{4\pi\varepsilon}\frac{\left(2\pi\sigma_0^2\right)^{3/2}}{2\sigma_0^2}\left[\mathrm{erf}(1) - \frac{2}{e\sqrt{\pi}}\right]. \tag{27}$$

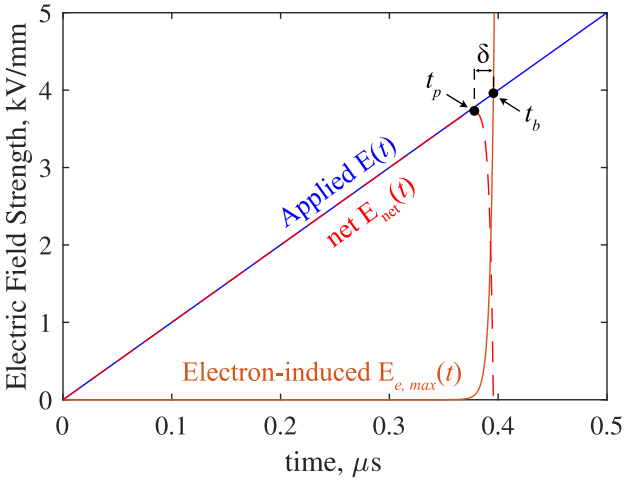

Fig. 2. Example of electric field strength over time for the applied ramp, max. electron-induced electric field, and net electric field. Indicated are: t_b – time for the electron-induced electric field and applied field to equal in magnitude, and t_p – time for the net field to reach a maximum. The difference, δ, is assumed negligible for the derivation of the closed-form approximation.

While the breakdown criterion is stated as (11), one may arrive at a good approximation of the solution by instead solving

$$\frac{\partial}{\partial t}\left[f \cdot \mathcal{D}t_p - C_0 \exp \mathcal{I}(t_p)\right] = f\mathcal{D} - C_0\frac{\partial \mathcal{I}(t_p)}{\partial t}\exp \mathcal{I}(t_p) = 0, \tag{28}$$

where it should be emphasised that t_p here is the time at which the *maximum electron-induced electric field rate of change equals the rate of change of the applied field*. This differs from t_b as defined in (11) which referred to the time that the fields became equal in magnitude. Equation (28) solves instead for the *peak of the net electric field*, and defines the breakdown time t_p. The time at which their rates match is equivalent to the time at which the net field begins to collapse, which happens so rapidly that $t_p \approx t_b$ is a reasonable approximation, as shown in Figure 2. Furthermore, if the initial electron-induced electric field is small (which would be the case assuming the avalanche was initiated from typical background ionisation levels), such that at time t_0^+ the applied field rises far more rapidly than the electron-induced electric field, $E_{e,max}(t_p)$ must necessarily be smaller than $E(t_p)$. Without loss of generality, the former may then be expressed as some fraction g of the applied field at this moment, $g \cdot E(t_p)$, allowing (28) to be rewritten as

$$t_p\frac{\partial \mathcal{I}(t)}{\partial t} = \frac{f}{g}. \tag{29}$$

The fraction g essentially becomes a fitting factor, however, the significance and selection of g is discussed further in Section III-C. Equation (29) can be shown to have the following closed form solutions

$$t_b = \frac{B_\alpha}{\mathcal{D}k_1\omega\left(\mathcal{D}\right)}, \qquad E_b = \frac{B_\alpha}{k_1\omega\left(\mathcal{D}\right)}, \qquad V_b = \frac{B_\alpha d}{k_1\omega\left(\mathcal{D}\right)}, \tag{30}$$

for the breakdown time, breakdown field, a nd i f applicable (developed between planar electrodes with separation d), the breakdown voltage. The function $\omega(\mathcal{D})$ has the definition

$$\omega(\mathcal{D}) = W\left[\frac{1}{k_1}\left(\frac{g\gamma_1}{f\mathcal{D}}\right)^{1/k_1}\right], \tag{31}$$

where W is the principal branch of the Lambert W (or product-log) function. Using fitting coefficients for Nitrogen from [8], Figure 3 plots t_b and E_b as a function of $\mathcal{D}$, the range of which was selected to be from 10^{10} to 10^{16} V/m·s, representing pulses peaking at tens to hundreds of kV within the nanosecond to hundreds of microsecond range, and in gaps of tens of millimeters separation. The time to breakdown expectedly decreases with increasing $\mathcal{D}$ owing to the quicker onset of ionisation and avalanche development. The breakdown field, E_b, was predicted to increase with increasing $\mathcal{D}$ following known experimental tendencies. The present model offers the following explanation of this behaviour. Under the zero diffusion and non-attaching assumption, both the applied field and electron-induced field are monotonically increasing functions with time. In the absence of significant pre-ionisation, the rate at which the electron-induced field can increase initially (at t_0^+) is always lower than $\mathcal{D}$. As such, the moment that the net field is maximised (moment of field collapse) is equal to the moment that the rate of change of the electron-induced field equals the rate of the rising applied field, $\mathcal{D}$. The mathematical equivalent to this statement is equation (28). With an increase to $\mathcal{D}$, the increase in the rate-of-rise of the applied field is greater than the increase to the rate-of-rise of the electron-induced field. This may further be confirmed based on the limit:

$$\lim_{\mathcal{D}\to\infty} \frac{\mathcal{D}t}{C_0 \exp \mathcal{I}(t)} = \infty. \tag{32}$$

Thus, despite higher values of $\mathcal{D}$ reducing t_b, the corresponding field at the moment that the rates are matched, E_b, becomes larger, as shown in Figure 3.

Based on (25), it may further be said that the above effect is due to the differing rates at which the ionisation coefficient, $\alpha(t)$, and electron mobility, $\mu_e(t)$, change with increasing electric field (and hence increasing $\mathcal{D}$ considering the present ramp field). From (14) and (15), ionisation activity increases with increased E, while mobility decreases. Their rates of change, however, are not equal, with the former increasing like $\exp(-1/E)$ and the latter decreasing with E^{-B_μ}. It is evident that the rate mobility decreases is faster than the rate that ionisation increases with increasing field. This limits the rate of change of $E_{e,max}$ with increasing $\mathcal{D}$ such that (32) becomes imposed.

C. The Nature of Parameter g

As defined in Section III-B, the fraction g represents the ratio between the magnitudes of the electron-induced field and applied field *at the moment that the net field reaches a maximum*. In general, g will be a function of $\mathcal{D}$, transport parameters, and of the initial field condition given by C_0. Figure 3 compares the closed form breakdown field solution

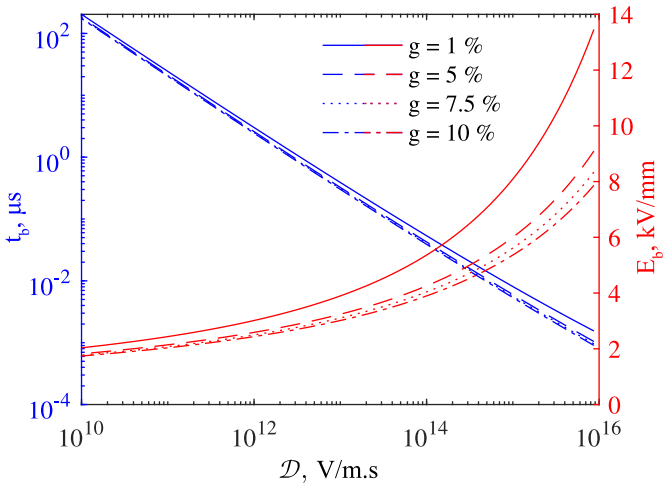

Fig. 3. The estimated breakdown time, t_b, and breakdown field magnitude, E_b, in the zero-diffusion, non-attaching limit (equations (30)), as a function of the rate of field rise, $\mathcal{D}$, and for g = 1, 5, 7.5, and 10 %. Transport data used represents Nitrogen.

of (30) for differing values of g across several magnitudes of the value $\mathcal{D}$ in Nitrogen. When C_0 is small, it was found that g values generally do not need to exceed $\sim 10\%$ to provide very good agreement between the closed form approximation and the full numerical solution, across a wide range of $\mathcal{D}$. This also suggests that the sensitivity of g to $\mathcal{D}$ may not be significant. This range of values indicate that the moment when the electron-induced field rate of change matches that of the applied field, its magnitude is generally $< 10\%$ of the applied field magnitude. Yet, the subsequent ionisation processes occur with such intensity that the field magnitudes become equal within a sufficiently short time for the assumption of $t_p \approx t_b$ to be appropriate. The value of g increases with higher initial fields, C_0, but the exact nature of this increase is not entirely clear given the strong coupling between t_b, C_0, and g. Clarification of this relationship is identified as an important future step for this model. It is remarked that in the absence of such an explanation, the value of g can be identified for a given model by choosing g such that the expressions (30) provide the best fit with the solutions to (7)–(10). The experimental comparisons within Section IV and subsequent discussion in Section V-A also suggest that g may have a strong dependency on diffusion, D_e.

IV. Model Validation and Comparison to Experimental Results

This section aims to compare the predicted results from the developed model to available experimental data found in literature. Section IV-A firstly focuses on the observed upward shift of Paschen's curve with higher rate of voltage rise, comparing the present mathematical solutions to simulated and experimental data. Then, Section IV-B follows to compare the predicted field-time scaling characteristics to a collation of experimental pulsed breakdown data, conducted under various common gases. Section IV-C compares the scaling of the estimated breakdown time as predicted by (30) with initiation

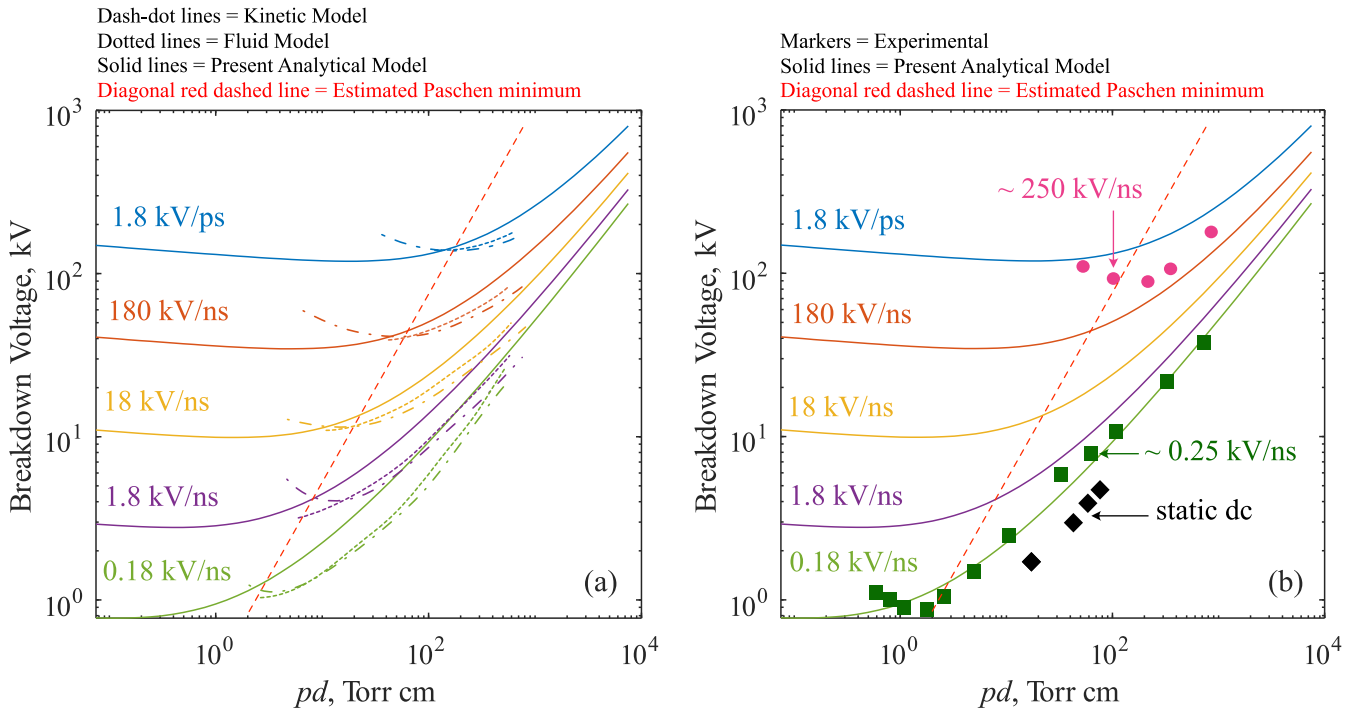

Fig. 4. Comparison of Paschen scaling curves for Nitrogen subject to ramp voltage as estimated by the present model to (left) fluid and kinetic simulation data from [21], (right) experimental data from [20] for atmospheric air (rod-plane gap, 1 cm), for different voltage ramps. Solid black diamond markers are the static breakdown case, and the red dashed line indicates the position of the estimated Paschen minimum and approximate limit where the model predictions begin to diverge.

times computed from hydrodynamic streamer simulations in [19]. For the model, the selection of initial electron density $n_0(t_0)$ and initial spread σ_0 was informed by approximate values for background ionisation densities, details of which can be found in Appendix B. It should also be noted that the experimental comparisons conducted here were to datasets that both used and did not use UV irradiation to provide starting electrons. Good agreement was found for a mixture of both types of data, but in general, it is difficult to decouple statistical effects from those arisen from the many other influencing factors that may be present, e.g., exact electrode configuration and gas conditions. Similarly, the initial conditions which define the initial cluster of electrons was chosen based on limited data; σ_0, $n_0(t_0)$ are both parameters with a high degree of uncertainty, particularly when considering the degree to which they may vary based on many scenario-dependent factors.

A. *Pulsed Paschen Curves*

The classical Paschen's Law established a relation between the breakdown voltage in gas to the pressure-distance (pd) product for breakdown under steady-state electric fields. The Paschen scaling for pulsed breakdown is known to deviate from the law in its original form, where the Paschen curve has been found to exhibit an upward shift with higher values of dV/dt both experimentally [20] and computationally [21]. This section verifies that the present model also exhibits pd scaling, while also showing that the upward shift with dV/dt can also be reasonably predicted using this method.

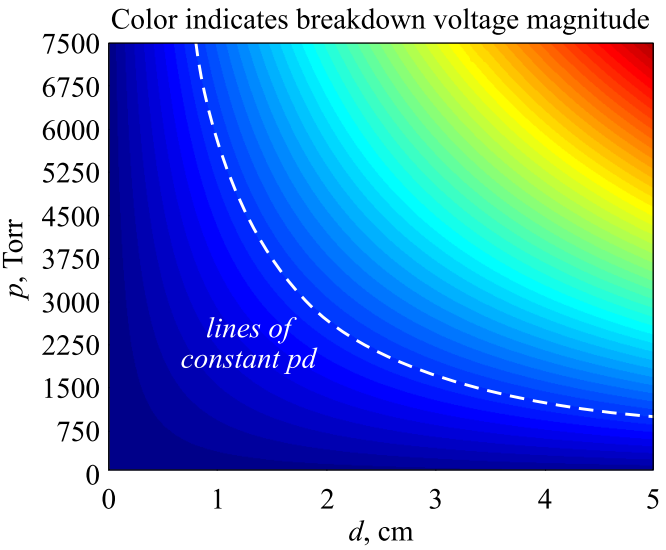

Fig. 5. Colour map of the full pd space from p up to 7500 Torr (1 to 10 bar), and d up to 5 cm. Colour indicates the breakdown voltage magnitude, which have equipotentials that align with curves of constant pd, satisfying pd scaling. No colour bar is shown as the exact value is unimportant here.

Consider Figure 4(a) and 4(b). The former shows the predictions of the present model compared to numerical modelling results in [21] using hydrodynamic and kinetic approaches. The latter compares these same predictions to experimental data from [20]. The conditions used here incorporate a ramp voltage rising up to 180 kV with various rise times resulting in the rates-of-rise indicated in the figure, applied to a gas gap of

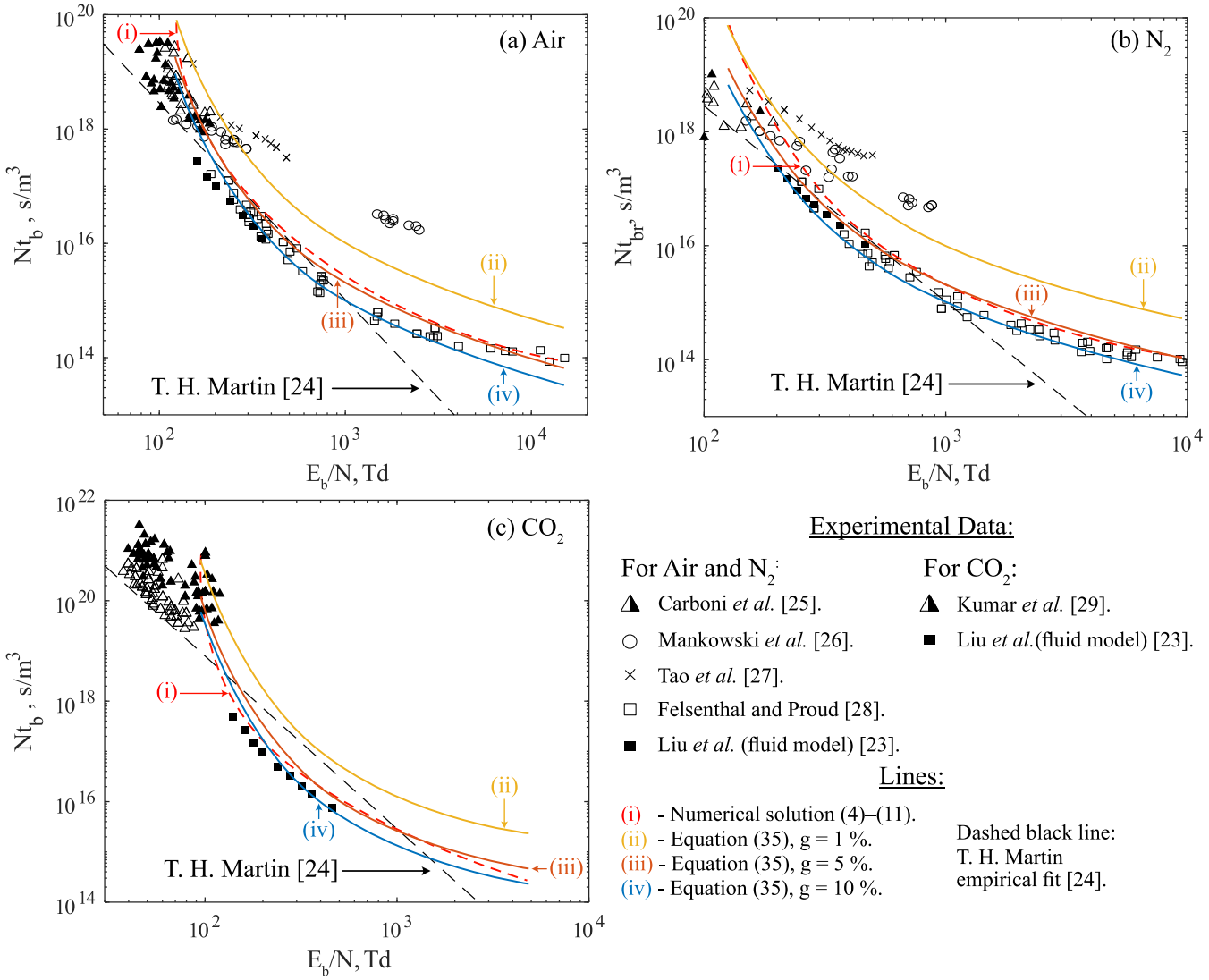

Fig. 6. Field-time scaling curves for (a) Air, (b) Nitrogen, (c) Carbon Dioxide, comparing experimental datapoints with the solution to the full numerical model and approximations at different values of parameter g. References enclosed in the shared figure legend. Note that selected data is formed of both those that were gathered with methods to render the statistical time lag negligible, and those that did not. Note also that the data of Kumar *et al.* was calculated from breakdown voltage values in [8] based on the average field strength across a non-uniform electrode gap.

1 cm filled with pure Nitrogen. Reasonable agreement between the present analytical approach, experimental data, and the far more complex numerical approaches has been observed—at least to the right of the Paschen minimum. Deviations begin to occur near the estimated location of the Paschen minimum indicated by the red dashed line. It is remarked that neither the present model nor fluid approaches from [21] could accurately recreate the left branch, suggesting significant changes in the breakdown mechanism within this region to do with kinetic or non-local effects. This is, however, left as a topic for future work. To confirm that the predicted breakdown voltages indeed exhibits scaling with pd, the pd space from $p = 0$ to 7500 Torr (1 to 10 bar) and d = 0 to 5 cm has been plotted in Figure 5, where the colour map is the predicted breakdown voltage (numerical values of which are unimportant to verify the pd scaling, thus have been omitted), for a constant value of $\mathcal{D}$. The dashed white line of Figure 5 indicates the lines of equipotential, which can be seen to align with lines described by $pd = c$ where c is a constant, confirming that the present model indeed exhibits scaling with the product pd. It should also be noted that the Lambert-W function, $W(x)$, as featured in (31) is asymptotic to $\ln x - \ln(\ln x)$ [22]. In which case, the closed form breakdown voltage from (30) can be further approximated to have the following proportionality:

$$V_b \propto \frac{pd}{\ln\left[f(p,d)\right) - \ln\left[\ln f(p,d)\right]}, \tag{33}$$

where k is a constant for a given gas and $\mathcal{D}$. Emphasis is placed on the form of (33), which bears a striking resemblance to that of the classical Paschen's law.

B. Breakdown Field-Time Scaling Characteristics

A method often employed to compare pulsed breakdown data is to plot the *field-time scaling* relationship of experimental breakdown results. This involves plotting the scaled breakdown time Nt_b against the reduced breakdown field

E_b/N, where N is the neutral gas density. In [23], numerous pulsed breakdown datasets were collated by the authors and compared in this way, which were also compared to a well-known empirical relation introduced by T. H. Martin [24]. The authors of [23] further compared datasets to the classical kinetic approach (Meek criterion), where the characteristic curve can be derived to be of the form

$$Nt_b = \frac{K}{\bar{\alpha}\mu_e} \cdot \frac{1}{E_b/N}, \tag{34}$$

where K is assumed to be 18. From (30), the scaling characteristic estimated by the present model can be written in a similar form:

$$Nt_b = \frac{B_\alpha^2}{k_1^2 \mathcal{D}\omega^2(\mathcal{D})} \cdot \frac{1}{E_b/N}, \tag{35}$$

but which now explicitly shows dependence on rate-of-rise, $\mathcal{D}$. In [23], equation (34) was shown to be in reasonable agreement with experimental data when evaluating (34) using field-dependent forms of $\bar{\alpha}$ and μ_e. However, as the classical approach did not explicitly consider $\mathcal{D}$, it offered little insight into the relationship it had with t_b and E_b, which the novel approach developed here was able to provide through (35) and through the previous analysis in Section III. Figures 6(a) to 6(c) presents a comparison between the experimental data collated in [23] to the scaling relationship (35) from the present model in air, Nitrogen, and CO_2. Data includes experiments conducted by Carboni *et al.* [25], Mankowski, Dickens, and Kristiansen [26], Tao *et al.* [27], Felsenthal and Proud [28], Kumar *et al.* [29], and fluid modelling data from Liu *et al.* [23]. Furthermore, both the solution to the full model (4)–(11) and its approximations in the zero-diffusion and non-attaching limit (30) have been plotted. To also show the sensitivity of the approximate scaling relation (35) to the parameter g, separate lines have been plotted for g of 1%, 5% and 10% of the applied field.

Overall, good agreement was found between the experimental data and the present model across a wide range of conditions. The approximations (30) also align with the full numerical solution very well, where a g value of 5–10% generally provided the best fit between the data and the full numerical approach.

C. Streamer Initiation Time

In Wong *et al.* [19], simulations of primary ionization waves initiated within air- and CO_2-filled needle-plane electrode gaps of 250 μm were conducted. The authors reported linear scaling of the observed wavefront initiation time with the inverse of rate of voltage rise (under ramp voltages), their results of which are reprinted here as Figure 7. Based on the closed-form approximations (30) developed in this work, it can be shown that the linear scaling of Figure 7 can be explained by, and is consistent with, the predictions of the present model.

Consider that the approximation for t_b according to (30) can be written as the proportionality

$$t_b \propto \frac{1}{\mathcal{D}\omega(\mathcal{D})}, \tag{36}$$

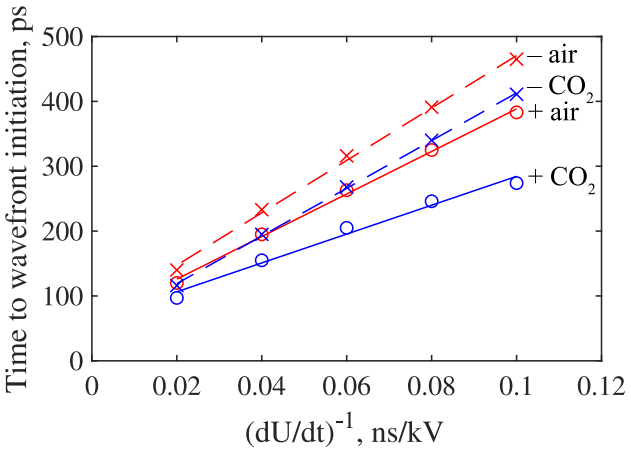

Fig. 7. Linear scaling of the streamer initiation time with $(dU/dt)^{-1}$ from [19], for positive and negative ramp voltages, in air and in CO_2. Image reproduced with permission from [19] under CC BY 4.0.

since B_α and k_1 are constant for a given gas. The function $\omega(\mathcal{D})$ from (31) is plotted over the range $10^{10} \leq \mathcal{D} \leq 10^{17}$ in the semi-log plot of Figure 8, from which there are two notable features. Firstly, the almost linear relation suggests that $\omega(\mathcal{D})$ can be well approximated by a relation of the form $\omega(\mathcal{D}) \approx k \log(\mathcal{D}/c)$, where c is independent of $\mathcal{D}$ but has units V/m·s to render the argument of the logarithm dimensionless. It is remarked that from (24) and (31), one may deduce that the parameter γ_1 satisfies this and has dimensions V/m·s, though this is not strictly necessary for the following analysis. Considering this, the proportionality $\omega(\mathcal{D}) \propto (\log \mathcal{D} - \log c)$ therefore applies. Secondly, comparison between the magnitudes of $\omega(D)$ values to the corresponding values of $\mathcal{D}$ shows clearly that $\omega(\mathcal{D})$ does not exhibit strong sensitivity to $\mathcal{D}$. This may further be confirmed by the derivative

$$\frac{\partial}{\partial \mathcal{D}} (\log \mathcal{D} - \log c) \propto \frac{1}{\mathcal{D}}. \tag{37}$$

It follows, therefore, that for the high $\mathcal{D}$ values within the ranges of interest (and as used in Wong *et al.* [19], which are in the approximate range of $10^{16} - 10^{17}$ V/m.s), the induced change to $\omega(\mathcal{D})$ over this range can effectively be assumed to be negligible. The proportionality (36) may hence be reduced to

$$t_b \propto \frac{1}{\mathcal{D}} \tag{38}$$

for sufficiently small variations in $\mathcal{D}$ since $\omega(\mathcal{D})$ can be treated as constant, in agreement with the scaling observed in [19] and in Figure 7.

V. Other Considerations

While the present model makes theoretical progress on the analysis of overstressed pulsed breakdown, the authors acknowledge that it is not yet a complete picture. This section briefly discusses a number of limitations of the presented approach and includes discussion of electron diffusion and positive ion inclusion.

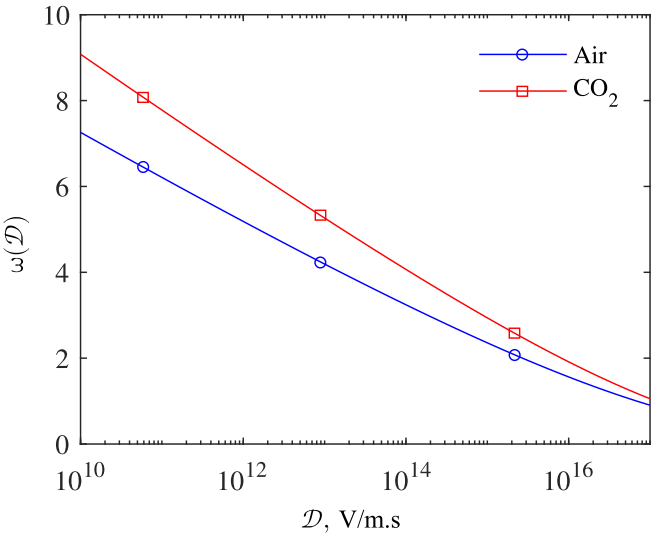

Fig. 8. The function $\omega(\mathcal{D})$ for air and CO_2 over several magnitudes of $\mathcal{D}$. The nearly linear character suggests $\omega(\mathcal{D}) \propto \log \mathcal{D}/c$ is a good approximation.

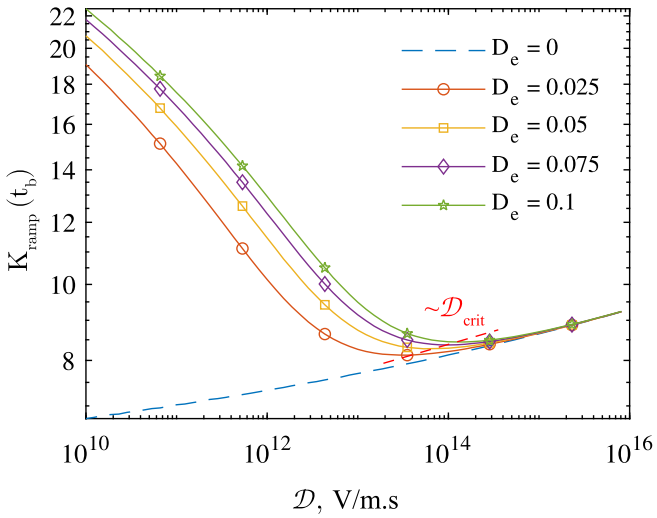

Fig. 9. Plot of the effective ionisation integral, K_{ramp}, at the time of breakdown estimated from the present model under ramp fields. Plotted as a function of $\mathcal{D}$, and for different values of diffusion constant D_e. Note that the dependence on D_e vanishes for higher $\mathcal{D}$ above some value $\mathcal{D}_{crit}$ which lies approximately beyond the minimum marked by the red dashed line.

A. *Diffusion may be Important for Pulsed Breakdown*

The equations (30) allowed the functional dependence of breakdown on $\mathcal{D}$ to be studied, a task which would have been highly nontrivial if D_e could not be assumed to be zero. There has been little exploration of the effects of electron diffusion for pulsed breakdown, which is generally assumed to be negligible based on the timescales involved. For example, the authors of [21] concluded from fluid simulations that the effects of diffusion may not be significant for breakdown on a rising slope. For constant applied fields, authors of [9] argued that diffusion should be included particularly for avalanches formed in low electric fields, where diffusive reduction could lead to substantial delays to the streamer transition moment. As diffusion is a time-dependent process, it follows that under a continuously rising background field, one should expect the parameter $\mathcal{D}$ to influence the extent that diffusive processes dominate.

Using (23), the value of the effective ionisation integral at breakdown, $K_{ramp}(t_b)$, as a function of $\mathcal{D}$ and at various values of diffusion coefficient, D_e, has been plotted in Figure 9. Also indicated is the zero-diffusion case. It is evident that K is not just dependent on D_e, but also exhibits a local minimum at some value of $\mathcal{D}$ for all cases with non-zero diffusion. The minimum can be explained by the time necessary for diffusion to become significant, where the region $\mathcal{D} < \mathcal{D}_{crit}$ is largely diffusion-dominant, since the voltage rises sufficiently slowly for diffusive effects to have tangible impacts on the peak magnitude of electrons forming the Gaussian. Where $\mathcal{D} > \mathcal{D}_{crit}$, breakdown is sufficiently quick such that diffusion has negligible effects. This is further evidenced by the convergence of all lines on Figure 9 as the effects of diffusion (irrespective of D_e) become unimportant.

While no closed solution for $\mathcal{D}_{crit}$ could be found, it can be shown from (23) that for electron diffusion to have a negligible impact on the breakdown evolution, the condition of

$$t_b \ll \frac{\sigma_0^2}{2D_e} \tag{39}$$

should be met. Equation (39) simply has the physical interpretation that the breakdown time must be far less than the diffusion time. This provides a condition separating where diffusion is likely to have strong influence on the breakdown, and where diffusion can be neglected. It is once again noted that D_e has been assumed constant in this work as a simplification, as such, (39) can only be considered an approximation. However, the conceptual discussion of the effects here should be equally applicable when D_e is field-dependent (and therefore also time-dependent). Based on (5), a more general condition should the effects of $D_e \rightarrow D_e(t)$ be considered would be

$$\int_{t_0}^{t_b} D_e(t)\ dt \ll \frac{\sigma_0^2}{2}, \tag{40}$$

which can be shown to equal (39) in the constant diffusion limit.

On the note of field-dependent diffusion, based on Figure 9 one should expect that equations (30) should incur significant inaccuracies for lower $\mathcal{D}$ due to the assumption that $D_e = 0$. In these cases, it is remarked that the choice of g should, to some degree, encapsulate the effects of diffusion, since it is a measure of the electron-induced field at the moment of field screening which itself is affected by diffusion. However, g was also assumed constant in this work (which according to Figure 6 appears to be somewhat suitable for a wide range of conditions), though it likely varies with the electron transport parameters, including diffusion. In a case where diffusion is also field- and time-dependent, a non-constant g may partially explain the larger discrepancies between the model and experiments observed in the low field regions

of Figure 6 (particularly for CO_2 which possesses a $D_e(E)$ relation that is much different from air and N_2). However, it is also remarked that this region is nearing the lower limit of validity for the parameter fitting expressions in this case, which may also introduce inaccuracies. In future, detailed investigation into the value of g and of its dependencies is of high priority.

B. Positive Ions

In this model, the effect of positive ions have not been incorporated. Even with (12) which can be numerically solved for the ion density as in Figure 1, the positive ion electric field was neglected since the ion density cannot be approximated by any simple geometry with accessible analytical solutions. Based on analysis of the ion trail in [9], consideration of the ion field would tend to increase the predicted breakdown strength since the ion field would act in opposition to the electron-induced field, thereby necessitating a longer time for either condition (11) or (28) to be satisfied. Also in [9], theoretical estimations indicated that the correction to the moment of transition when considering the ion field may be negligible for breakdown occurring over short timescales, or when diffusion can be ignored. It is therefore expected that inclusion of the ion field may not significantly change the presented estimations. On the basis of the analysis relating to diffusion of Section V-A, the positive ion field may become important under configurations where the ratio between the ionisation length and diffusion length becomes non-negligible [9]. Its inclusion, however, would likely prohibit the closed-form approximations of this work to be developed. Given the potential scope of this inclusion, to consider other charged species is left as an aspect for future work. This model also does not consider effects of nearby boundaries such as electrodes or other dielectrics, therefore also forgoing the effects of secondary electron sources.

VI. Conclusion

In this work, the diffusion-corrected Meek criterion developed in [9] has been further advanced for the specific purpose of analysing overstressed breakdown on a rising slope. The approach is based on the simplified transport of a Gaussian distributed electron cloud combined with semi-empirical fitting functions for electron transport parameters. A set of equations have been formulated to identify the moment of avalanche-to-streamer transition under an arbitrary time-dependent field. Further progress was made by analysing the specific case of a linearly increasing applied field with defined rate-of-rise. It has been shown that the ionisation growth rate under these conditions follow that of the upper incomplete gamma function, describing the slow initial rise but rapid screening of the applied field as the avalanche grows in size. Furthermore, in the non-attaching and non-diffusive limit, it was shown that approximations for the time-to-breakdown, t_b, and breakdown field strength, E_b, can be found as explicit functions of the rate-of-field-rise, $\mathcal{D}$, using the Lambert-W (product-log) function. Mathematical analysis explains the trend of increasing breakdown strength with increasing dV/dt as a result of the differing rates of electron-induced field rise compared to the rate-of-rise of the applied field. This is further linked to the mismatched rates at which the ionisation coefficient and electron mobility can change with increased rate-of-rise.

Model predictions have been validated against simulated and experimental data drawn from literature. It was demonstrated that the model exhibits pd scaling and is able to recreate the upward shift of the Paschen curve for increasing rise time. It also adequately predicts the field-time scaling characteristic for pulsed breakdown in a comparison to numerous experimental datasets, presented alongside a new characteristic scaling relation with explicit inclusion of the rate-of-rise. Based on fluid simulations of primary ionisation wavefronts, the developed model also explains an observed linear scaling of the streamer initiation time with the reciprocal of the rate-of-rise. The importance of diffusion on breakdown on a rising slope has also been analysed, finding that the influence of electron diffusion is dependent on the rate-of-rise. An approximate condition separating the diffusion-dominant region and where diffusion can be neglected has been proposed. The developed model therefore advances the theoretical knowledge of fundamental electron transport and avalanche development processes under the fast-rising overstressed breakdown regime. This is of particular importance to the design of current and future pulsed power systems and components.

This study has also identified a number of areas which would benefit from further theoretical and/or experimental study, listed below:

- Under what conditions does the positive ion field have sufficient impact on the avalanche development to warrant inclusion?
- What effects would the inclusion of time-dependent diffusion, $D_e \rightarrow D_e(t)$, have on the predicted breakdown characteristics and scaling curves? Can it explain the discrepancies observed at lower values of $\mathcal{D}$?
- The functional dependencies of g—it is believed that there is unexplored significance to this value. It may be an important parameter for the further characterisation of pulsed breakdown.
- What processes to the left of the Paschen minimum result in the deviations observed from the present model and fluid simulations?
- Can a similar approach be used to analyse certain non-uniform field configurations, where the avalanche may effectively experience a time-varying field due to its transport through a region where the there exist a spatially-varying electric field?

Appendix A
Diffusion of Gaussian from Fick's Second Law using Green's Function

Consider Fick's second law, canonically written

$$\frac{\partial n}{\partial t} = D\vec{\nabla}^2 n \tag{41}$$

where n is the concentration (density) and D is the (assumed isotropic) diffusion coefficient. In the real-space $\mathbb{R}^3$, the Green's function for (41) reads [33]

$$u(\vec{\mathbf{x}},t) = \frac{1}{(4\pi Dt)^{3/2}} \int_{\mathbb{R}^3} g(\vec{\mathbf{y}}) \cdot \exp\left[-\frac{|\vec{\mathbf{x}}-\vec{\mathbf{y}}|^2}{4Dt}\right] d^3\vec{\mathbf{y}}, \quad (42)$$

where $g(\vec{\mathbf{y}})$ is the initial condition

$$g(\vec{\mathbf{x}}) = g_0(t_0)\exp\left(-\frac{|\vec{\mathbf{x}}|^2}{2\sigma_0^2}\right). \quad (43)$$

It follows that

$$\begin{aligned} u(\vec{\mathbf{x}},t) &= \frac{g_0(t_0)}{(4\pi Dt)^{3/2}} \int_{\mathbb{R}^3} \exp\left\{-\left[\frac{\vec{\mathbf{y}}^2}{2\sigma_0^2} + \frac{|\vec{\mathbf{x}}-\vec{\mathbf{y}}|^2}{4Dt}\right]\right\} d^3\vec{\mathbf{y}} \\ &= \exp\left(-\frac{|\vec{\mathbf{x}}|^2}{(2\sigma_0^2+4Dt)}\right) \\ &\times \exp\left[-\frac{(2\sigma_0^2+4Dt)}{2\sigma_0^2(4Dt)}\left|\vec{\mathbf{y}} - \frac{2\sigma_0^2}{(2\sigma_0^2+4Dt)}\vec{\mathbf{x}}\right|^2\right], \end{aligned} \quad (44)$$

where one may use the change of variable

$$\begin{aligned} \vec{\mathbf{z}} &= \sqrt{\frac{2\sigma_0^2+4Dt}{2\sigma_0^2(4Dt)}}\left(\vec{\mathbf{y}} - \frac{2\sigma_0^2}{2\sigma_0^2+4Dt}\vec{\mathbf{x}}\right), \\ d^3\vec{\mathbf{z}} &= \left[\frac{2\sigma_0^2(4Dt)}{2\sigma_0^2+4Dt}\right]^{3/2} d^3\vec{\mathbf{y}}, \end{aligned} \quad (45)$$

to simplify the integral. The integrand therefore collapses to one single exponential over $d^3\vec{\mathbf{z}}$, the result of which is $\pi^{3/2}$. It remains that the solution $u(\vec{\mathbf{x}},t)$ becomes

$$\begin{aligned} &u(\vec{\mathbf{x}},t) \\ &= \frac{g_0(t_0)}{(4\pi Dt)^{3/2}}\exp\left(-\frac{|\vec{\mathbf{x}}|^2}{2\sigma_0^2+4Dt}\right)\left[\frac{2\sigma_0^2(4Dt)}{2\sigma_0^2+4Dt}\right]\pi^{3/2} \\ &= g_0(t_0)\frac{\pi^{3/2}}{(4\pi Dt)^{3/2}}\frac{\left[2\sigma_0^2(4Dt)\right]^{3/2}}{(2\sigma_0^2+4Dt)^{3/2}}\exp\left(-\frac{|\vec{\mathbf{x}}|^2}{2\sigma_0^2+4Dt}\right) \\ &= g_0(g_0)\frac{(2\pi\sigma_0^2)^{3/2}}{(2\pi\sigma_0^2+4\pi Dt)^{3/2}}\exp\left(-\frac{|\vec{\mathbf{x}}|^2}{2\sigma_0^2+4Dt}\right), \end{aligned} \quad (46)$$

which is identical to the result (5) with $g_0(t_0) \to n_0(t)$, $|\vec{\mathbf{x}}| \to r$, and $D \to D_e$. Note that this solution is applicable also the the case when $D \to D(t)$, where the substitution

$$Dt \to \int_{t_0}^{t} D(t')\ dt' \quad (47)$$

need only be made, as long as diffusion remains isotropic.

Appendix B
Selection of Initial Conditions

Throughout the present work, the initial conditions for the electron cloud, $n_0(t_0)$ and σ_0 have been kept constant; their values determined by estimates of typical background ionisation levels. Based on an estimated uniform background electron density of n_a = 10^9 m^{-3} [30], a peak value of $n_0(t_0)$ of 10^{13} m^{-3} was chosen, which was also informed by its use in various numerical modelling studies [31]. Considering that this is a peak value (representing a localised packet of electrons) and not uniform, this value could conceivably be driven by ionisation from background sources, or remaining from a previous discharge within a laboratory setting [32].

The choice of the initial deviation parameter, $\sigma_0 = 10^{-4}\,\mathrm{m}$ was based on approximate dimensions of simulated electron avalanches in [18] using particle kinetic methods. Since this work considered an initial *density* of electrons to facilitate the incorporation of avalanche initiation from multiple electrons (or multiple localised avalanches that merge and act effectively as a single, larger, avalanche), one may calculate the total number of electrons based on the assumed value of $n_0(t_0)$ by

$$N_e = \iiint_{\mathbf{S}} n_e(r,t_0)\ d^3\mathbf{S}, \quad (48)$$

where the volume integral over the three-dimensional sphere $\mathbf{S}$ is the total electron number in the Gaussian. An assumed value for σ_0 on the order of 10^{-4} meters corresponds to N_e on the order of 10^2, which was sufficiently low and deemed feasible as a reasonable initial condition. Within the assumed uniform background density of $10^9\,\mathrm{m}^{-3}$, a similar number of electrons would be expected in a volume of $(\approx 5\,\mathrm{mm})^3$.

References

[1] J. S. Townsend, The theory of ionization of gases by collision, London, Constable, 1910.

[2] F. Paschen, "Ueber die zum Funkenuebergang in Luft, Wasserstoff und Kohlensaeure bei verschiedenen Drucken erforderliche Potentialdifferenz," *Ann. Phys.*, vol. 273, no. 5, pp. 69-75, 1889.

[3] J. M. Meek, "A Theory of Spark Discharge," *Phys. Rev.*, vol. 57, no. 8, p. 722, Apr. 1940.

[4] L. B. Loeb and J. M. Meek, "The Mechanism of Spark Discharge in Air at Atmospheric Pressure. I," *J. Appl. Phys.*, vol. 11, no. 6, pp. 438-447, Jun. 1940.

[5] L. B. Loeb and J. M. Meek, "The Mechanism of Spark Discharge in Air at Atmospheric Pressure. II," *J. Appl. Phys.*, vol. 11, no. 7, pp. 459-474, Jul. 1940.

[6] L. B. Loeb and J. M. Meek, The Mechanism of the Electric Spark, Standford University Press, 1941.

[7] H. Raether, Electron Avalanches and Breakdown in Gases, London Butterworths, 1964.

[8] T. Liu, I. V. Timoshkin, S. J. MacGregor, M. P. Wilson, M. J. Given, N. Bonifaci, and R. Hanna, "Field-Time Breakdown Characteristics of Air, N_2, CO_2, and SF_6,", *IEEE Trans. Plasma Sci.*, vol. 48, no. 10, pp. 3321-3331, Oct. 2020.

[9] C. Montijn and U. Ebert, "Diffusion correction to the Raether-Meek criterion for the avalanche-to-streamer transition," *J. Phys. D: Appl. Phys.*, vol. 39, no. 14, p. 2979, Jun. 2006.

[10] R. T. Waters and W. B. Stark, "Characteristics of the stabilized glow discharge in air," *J. Phys. D: Appl. Phys.*, vol. 8, no. 4, p. 416, 1975.

[11] W. S. Zaengl and K. Petcharaks, Application of Streamer Breakdown Criterion for Inhomogeneous Fields in Dry Air and SF6. In: L. G. Christophorou and D. R. James, Gaseous Dielectrics VII, Springer, Boston, MA, 1994.

[12] L. Niemeyer, "A generalized approach to partial discharge modeling," *IEEE Trans. Dielectr. Electr. Insul.*, vol. 2, no. 4, pp. 510-528, Aug. 1995.

[13] J. J. Lowke and F. D'Alessandro, "Onset corona fields and electrical breakdown crtieria," *J. Phys. D: Appl. Phys.*, vol. 36, no. 21, p. 2673, Oct. 2003.

[14] G. V. Naidis, "Conditions for inception of positive corona discharges in air," *J. Phys. D: Appl. Phys.*, vol. 38, no. 13, p. 2211, Jun. 2005.

[15] P. N. Mikropoulos and V. N. Zagkanas, "Threshold inception conditions for positive DC corona in the coaxial cylindrical electrode arrangement under variable atmospheric conditions," *IEEE Trans. Dielectr. Electr. Insul.*, vol. 22, no. 1, pp. 278-286, Feb. 2015.

[16] A. Chirokov, A. Gutsol, and A. Fridman, "Atmospheric pressure plasma of dielectric barrier discharges," *Pure Appl. Chem.*, vol. 77, no. 2, pp. 487-495, 2005.
[17] A. Sun, C. Huo, and J. Zhuang, "Formation mechanism of streamer discharges in liquids: a review," *High Voltage*, vol. 1, no. 2, pp. 75-80, Jul. 2016.
[18] A. P. Jovanovic, S. N. Stamenkovic, M. N. Stankov, and V. L. Markovic, "Monte Carlo simulation of electron avalanches and avalanche size distributions in methane," *Contrib. to Plasma Phys.*, vol. 59, no. 3, pp. 272-283, Mar. 2019.
[19] T. Wong, I. Timoshkin, S. MacGregor, M. Wilson, and M. Given, "A computational study on the effects of fast-rising voltage on ionization fronts initiated in sub-mm air and CO_2 gaps," *Sci. Rep.*, vol. 14, no. 1184, Jan. 2024.
[20] L. Babich, High-energy Phenomena in Electric Discharges in Dense Gases: Theory, Experiment and Natural Phenomena, Futurepast, 2003.
[21] D. Levko, R. R. Arslanbekov, and V. I. Kolobov, "Modified Paschen curves for pulsed breakdown," *Phys. Plasmas*, vol. 26, no. 6, p. 064502, Jun. 2019.
[22] R. M. Corless, G. H. Gonnet, D. E. G. Hare, D. J. Jeffrey, and D. E. Knuth, On the Lambert W Function in *Adv. Comput. Math.*, vol. 5, pp. 329-359, Springer, 1996.
[23] T. Liu, I. Timoshkin, M. P. Wilson, M. J. Given, and S. J. MacGregor, "The Nanosecond Impulsive Breakdown Characteristics of Air, N_2, and CO_2 in a Sub-mm Gap," *Plasma*, vol. 5, no. 1, pp. 12-29, Dec. 2021.
[24] T. H. Martin, "An empirical formula for gas switch breakdown delay," in 7th Pulsed Power Conf., Monterey, CA, USA, Jun. 1989.
[25] V. Carboni, H. Lackner, D. Giri, and J. Lehr, "The breakdown fields and risetimes of select gases under the conditions of fast charging ($\tilde{2}$0 ns and less) and high pressures (20-100 atmospheres)," in 28th IEEE Int. Conf. Plasma Sci. and 13th IEEE Int. Pulsed Power Conf., Las Vegas, NV, USA, Jun. 2001.
[26] J. Mankowski, J. Dickens, and M. Kristiansen, "High voltage subnanosecond breakdown," *IEEE Trans. Plasma Sci.*, vol. 26, no. 3, pp. 874-881, Jun. 1998.
[27] S. Tao *et al*., "An experimental investigation of repetitive nanosecond-pulse breakdown in air," *J. Phys. D: Appl. Phys.*, vol. 39, no. 10, p. 2192, May 2006.
[28] P. Felsenthal and J. M. Proud, "Nanosecond-Pulse Breakdown in Gases," *Phys. Rev.*, vol. 139, no. 6A, p. A1796, Sep. 1965.
[29] S. Kumar, T. Huiskamp, A. J. M. Pemen, M. Seeger, J. Pachin, and C. M. Franck, "Electrical Breakdown Study in CO_2 and CO_2-O_2 Mixtures in AC, DC and Pulsed Electric Fields at 0.2-1 MPa Pressure," *IEEE Trans. Dielectr. Electr. Insul.*, vol. 28, no. 1, pp. 158-166, Feb. 2021.
[30] S. Pancheshnyi, "Role of electronegative gas admixtures in streamer start, propagation and branching phenomena," *Plasma Sources Sci. Technol.*, vol. 14, no. 4, p. 645, Aug. 2005.
[31] B. Bagheri, J. Teunissen, and U. Ebert, "Simulation of positive streamers in CO_2 and in air: the role of photoionization or other electron sources," *Plasma Sources Sci. Technol.*, vol. 29, no. 12, p. 125021, Dec. 2020.
[32] S. Nijdam, G. Wormeester, E. M. van Veldhuizen, and U. Ebert, "Probing background ionization: positive streamers with varying pulse repetition rate and with a radioactive admixture," *J. Phys. D: Appl. Phys.*, vol. 44, no. 45, p. 455201, Oct. 2011.
[33] D. G. Duffy, Green's Functions With Applications, 2nd Ed., Chapman and Hall/CRC, New York, 2015.

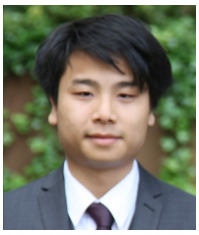

Timothy Wong (Member, IEEE) received the M.Eng degree in electrical and mechanical engineering with international study from The University of Strathclyde, Glasgow, U.K., in 2020. He is currently pursuing the degree of Ph.D. in electronic and electrical engineering and is a research assistant at the University of Strathclyde, Glasgow, U.K., with the High Voltage Technologies research group. His research interests include mathematical modelling of physical phenomena relevant to novel pulsed power and plasma technology, encompassing impulse-driven electrical breakdown, nonthermal plasma processes, and the optimisation of pulsed power systems. He was the recipient of the IMechE student award in 2020 where he is an Associate Member, and is currently a member of the IEEE Dielectrics and Electrical Insulation society (DEIS) and the IEEE Nuclear and Plasma Sciences society (NPSS). He is also a member of the IET. He was the recipient of the DEIS Best Student Presentation Award at the 14th Universities High Voltage Network Colloquium in 2022, and was further awarded the NPSS Outstanding Student Paper Award at the 24th IEEE International Pulsed Power Conference in 2023. In 2024, he received the NPSS Graduate Scholarship Award and was a recipient of an EPSRC Doctoral Prize Research Fellowship.

Igor Timoshkin (Senior Member, IEEE) received the degree in physics from Moscow State University, Moscow, Russia, in 1992, and the Ph.D. degree from the Imperial College of Science, Technology, and Medicine (ICSTM), London, U.K., in 2001. He was a researcher at Moscow State Agro Engineering University, Moscow, and then at the Institute for High Temperatures of Russian Academy of Sciences, Moscow. In 1997 he joined ICSTM. Then he joined the department of Electronic and Electrical Engineering, University of Strathclyde, Glasgow, U.K., in 2001, where he became a Reader in 2016. His research interests include dielectric materials, pulsed power, transient spark discharges, environmental applications of non-thermal plasma discharges. Dr. Timoshkin was a Voting Member of the Pulsed Power Science and Technology Committee in the IEEE Nuclear and Plasma Science Society (2017-2021); currently he is a member of International Advisory Committee of the IEEE Conference on Dielectric Liquids, a member of the International Scientific Committee of the Gas Discharges and Their Applications Conference, and a Subject Editor of IET Nanodielectrics.

Scott MacGregor (Senior Member, IEEE) received the B.Sc. and Ph.D. degrees from the University of Strathclyde, Glasgow, U.K., in 1982 and 1986, respectively. He was a Pulsed-Power Research Fellow in 1986 and a Lecturer in pulsed-power technology in 1989. In 1994, he became a Senior Lecturer, with a promotion to Reader and a Professor of High Voltage Engineering, in 1999 and 2001, respectively. In 2006 and 2010, he became the Head of the Department of Electronic and Electrical Engineering and the Executive Dean of the Faculty of Engineering, and has been the Vice-Principal with the University of Strathclyde, since 2014. His current research interests include high-voltage pulse generation, high-frequency diagnostics, highpower repetitive switching, high-speed switching, electronic methods for food pasteurization and sterilization, the generation of high-power ultrasound (HPU), plasma channel drilling, pulsed-plasma cleaning of pipes, and the stimulation of oil wells with HPU. Prof. MacGregor was a recipient of the 2013 IEEE Peter Haas Award. He was an Associated Editor of the IEEE Transactions of Dielectrics and Electrical Insulation in 2015.

Mark Wilson (Member, IEEE) was born in Stranraer, Scotland, in 1982. He received the B.Eng. (with honours), M.Phil., and Ph.D. degrees in electronic and electrical engineering from the University of Strathclyde, Glasgow, U.K., in 2004, 2007, and 2011, respectively. He is presently based in the High Voltage Technologies research group at the University of Strathclyde, where his research interests include interfacial surface flashover, nanodielectrics, and the practical applications of high-power ultrasound, corona discharges, and pulsed electric fields. Mark is a member of the IEEE Nuclear and Plasma Science Society, from whom he received a Graduate Scholarship Award in 2011, the IEEE Dielectrics and Electrical Insulation Society, and the IET.

Martin Given (Senior Member, IEEE) received the B.Sc. degree in physics from the University of Sussex, Brighton, U.K., in 1981, and the Ph.D. degree in electronic and electrical engineering from the University of Strathclyde, Glasgow, U.K., in 1996. He is currently a Senior Lecturer with the Department of Electronic and Electrical Engineering, University of Strathclyde. His current research interests include ageing processes and condition monitoring in solid and liquid insulation systems, highspeed switching, and pulsed power.